RSC Advances

ROYAL SOCIETY OF CHEMISTRY

www.rsc.org/advances

Journal Name

ARTICLE

DMSO-based PbI_2 precursor with $PbCl_2$ additive for high efficient perovskite solar cells fabricated at low temperature

Received 00th January 20xx,
Accepted 00th January 20xx

DOI: 10.1039/x0xx00000x

www.rsc.org/

Zhirong Zhang,[a,b] Xiaopeng Yue,[a,c] Dong Wei,[a] Meicheng Li,[a,*] Pengfei Fu,[a] Bixia Xie,[a] Dandan Song[a] and Yingfeng Li[a]

Using dimethylsulfoxide (DMSO)-based PbI_2 precursor solution and employing $PbCl_2$ as an additive, organolead halide perovskites films were fabricated via sequential solution deposition process. It is found that $PbCl_2$ additive in DMSO system dramatically improves the properties of the resultant perovskite films, including the crack-free morphology and enhanced light absorption, while its crystalline structure is not altered. Under the condition of 30 mol % $PbCl_2$ doping, the films exhibit a high uniformity and an optimum light harvesting capability; as-prepared solar cells achieve the highest power conversion efficiency of 14.42%, which is 36.3% higher than that of pure PbI_2-based one. The cells employ a nanocrystalline of rutile titania as the contact layer deposited by a chemical bath deposition method, contributing to preparing the devices at a low temperature less than or equal to 100 ℃.This work provides a simple, low-cost but effective strategy to improve the power efficiency of the perovskite solar cells.

Introduction

Organolead halide perovskites are a promising, low cost, easily synthesized set of materials that exhibits excellent optical and electrical properties [1–7]. The methylammonium trihalide perovskite-based solar cells (PSCs) have been reported widely [8–16], and a recent study has demonstrated the power conversion efficiency (PCE) approximate to 20% from a planar heterojunction PSCs [17]. The most commonly used perovskite is $CH_3NH_3PbI_3$ ($MAPbI_3$), whose morphology and crystal structure are of great impact on the performance of the photovoltaic devices [18,19]. The incorporation of chloride in precursor solution is an important technique to ameliorate the surface morphology and the optoelectronic properties of the perovskite films [2,20–26], and the resultant are often referred as the mixed-halide perovskite $CH_3NH_3PbI_{3-x}Cl_x$ ($MAPbI_{3-x}Cl_x$) (the name $MAPbI_3$ will be used throughout this article for some reason). While, several studies showed that there is only a negligible amount of chloride phase in the final perovskite films with the confirmation of XRD and XPS analysis [27,28], which is unexpected more or less. Although the action mechanism of chlorine in the formation process of ammonium lead halide perovskites has been investigated by several studies [29–31], it still remains controversial. Anyway, its beneficial effects which involve increasing the carrier lifetime and diffusion length, reducing the resistivity of perovskite film, etc. are widely recognized [2,21,32]. Various approaches of chloride doping have been reported, for instance, mixing $CH_3NH_3I_3$ and $PbCl_2$ with a molar ratio of 3:1 [1], incorporating CH_3NH_3Cl or NH_4Cl into a typical precursor mixture of PbI_2 and CH_3NH_3I [20,22]. In almost all studies, N, N-dimethylformamide (DMF) is used as the solvent for preparing PbI_2 precursor, which not only leads to a rapid crystallization of PbI_2 with a large and random grain sizes (the large crystal grains tend to form a perovskite film with lots of pinholes), but also inhibits the complete conversion of inner PbI_2 to $MAPbI_3$; while, both of these are detrimental to the performance of the photovoltaic devices [8,33,34]. Seok's group and Han's group reported, respectively, that by using the strongly coordinative solvent DMSO, a highly uniform perovskite film with no residual PbI_2 is obtained owing to the formation of PbI_2–DMSO complex and its retardant crystallization [34,35].

Inspired by this, we employ $PbCl_2$ as additive in DMSO-based PbI_2 precursor and prepare $MAPbI_3$ films via sequential solution deposition process, by which the advantages of both doping chloride and using DMSO as solvent as mentioned above are combined. Meanwhile, the solubility of $PbCl_2$ in DMSO is much higher than that in DMF, which would be beneficial for improving the uniformity of the perovskite films. The experiment results show that $PbCl_2$ in DMSO system dramatically impact the quality and the light absorption of the resultant perovskite films, while the crystalline structure is not altered. As-prepared PSCs (with a structure of FTO/nanocrystalline TiO_2/$MAPbI_3$/Spiro-MeOTAD/Au) exhibit an average PCE of 13.35%, which is 34.7 per cent higher than that of the pure PbI_2-based one. It is worth mentioning that our cells were prepared at a low temperature less than or equal to 100 ℃, owing to employing a nanocrystalline of rutile titania (NRT) as the contact layer, which is deposited by chemical bath deposition

[a] State Key Laboratory of Alternate Electrical Power System with Renewable Energy Sources, North China Electric Power University, Beijing, 102206, China.
[b] School of Physics and Electromechanical Engineering, HeXi University, Zhangye Gansu, 734000, China.
[c] Key Laboratory of Resource Exploration Research of Hebei Province, Hebei University of Engineering, Handan Hebei, 056038, China.
* Corresponding author information: E-mail: mcli@ncepu.edu.cn; Fax: +86 10 6177 2951; Tel: +86 10 6177 2951.
Electronic Supplementary Information (ESI) available: See DOI: 10.1039/x0xx00000x

method [36]. This work provides a simple but effective approach to fabricate high-performance PSCs at low temperature.

Experimental

Materials

Unless stated otherwise, all materials were purchased from Sigma-Aldrich or Acros Organics and used as received. Spiro-MeOTAD was purchased from Merck KGaA. FTO glasses of 2.2 mm thickness and less than 20 Ω sq^{-1}. were purchased from Pilkington. CH_3NH_3I was prepared as reported elsewhere [1]. Methylamine (CH_3NH_2) solution 33 wt% in absolute ethanol and hydroiodic acid (HI) 57 wt % in water were stirred at 0 ℃ for 2 hours. Typical quantities were 24 mL methylamine and 10 mL HI with 100 mL ethanol. The resultant solution was evaporated to give a white precipitate, then washed with diethyl ether and dried under vacuum and used for the following step without further purication.

Fabrication of photovoltaic devices

Devices were fabricated on FTO glass sheets. Initially FTO was etched with zinc powder and HCl (2 M) to obtain the required electrode pattern, for preventing shunting upon contact with measurement pins. The sheets were then washed with soap (2% Hellmanex in water), deionized water, acetone, and methanol and finally treated under oxygen plasma for 15 min to remove the last traces of organic residues. NRT contact layer was prepared as reported in literature procedures [36]. The substrates were immersed in 200 mM aqueous solution of titanium tetrachloride ($TiCl_4$) in a closed vessel and kept in a water bath at 70 ℃ for 1 hour, then rinsed with deionized water and ethanol.

To prepare the perovskite layers, 1 M PbI_2 solution in DMF or DMSO (doping a varying dosage of $PbCl_2$) was spin-coated at 4,000 r.p.m. for 30 s, then the substrates were dipped into CH_3NH_3I solution dissolved in 2-propanol (10 mg mL^{-1}) for 10 min and then annealed at 100 ℃ for 30 min. A hole-transporting layer (HTL) was then deposited by spin-coating. The spin-coating formulation was prepared by dissolving 72.3 mg spiro-MeOTAD, 28.8 µL 4-tert-butylpyridine (TBP, 99%), 17.5 µL lithium-bis(trifluoromethylsulphonyl)imide (Li-TFSI, 99.95%) solution (520mg Li-TFSI in 1 mL acetonitrile) in 1 mL chlorobenzene (99.8%). The devices were then left overnight in air for full oxidization of HTL. Finally, 100 nm gold electrodes were deposited on top of the HTL through a metal shadow mask via magnetron sputtering with a low current intensity of 5mA, to finish the fabrication. The active area of cells was defined as 0.1 cm^2. Only the preparation of perovskite layers was carried out in glove box with humidity levels of less than 5%, and the other steps were conducted in ambient atmosphere with humidity of less than 30%.

Measurement methods

X-ray diffraction (XRD) spectra were measured with a Panalytical X'Pert Pro x-ray diffractometer using Cu K_α radiation at 40 kV and 40 mA. A field emission scanning electron microscope (SEM, HITACHI UHR FE-SEM SU8200) was used to acquire SEM images. The optical absorption of perovskite films were studied by Shimadzu Ultraviolet-Visible (UV-vis) spectrophotometer (UV 2600). The current density-voltage (*J-V*) curves were measured using a digital source meter (Keithley Model 2400) to apply an external potential bias to the solar cells and measuring the generated photocurrent. The emission spectrum from a 450 W xenon lamp was matched to the standard AM1.5G using a Schott K113 Tempax sunlight filter (Praezisions Glas & Optik GmbH). The exact light intensities of the measurements were determined using a calibrated Si diode as reference.

Results and Discussions

Analysis of X-Ray diffractometer

Firstly, we investigated the effect of the precursor solutions on crystalline structure of the perovskite film by XRD analysis. For comparison, $MAPbI_3$ films were prepared (on glass substrates) by using various precursor solutions with slight differences in solvent or molar ratio of $PbCl_2$ additive (summarized in Table 1), and the XRD patterns of these films are showed in Figure 1.

Table 1. Fabrication parameters of the perovskite films prepared by various precursor solutions

Label of film	Solvent	PbI_2 (mol %)	$PbCl_2$ (mol %)
a	DMF	100	0
b	DMSO	100	0
c	DMSO	90	10
d	DMSO	70	30
e	DMSO	50	50
f	DMSO	30	70
g	DMSO	10	90

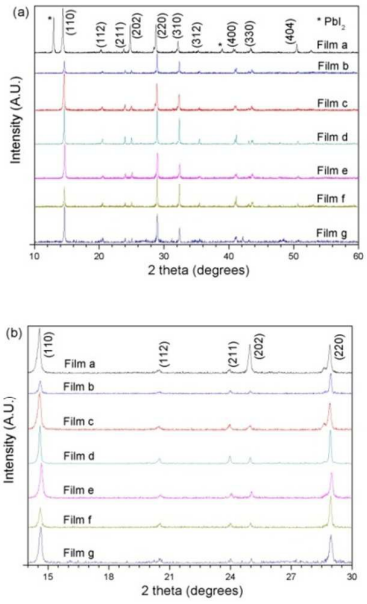

Fig. 1 (a) XRD patterns for perovskite films prepared with various precursor solutions. (b) Magnified views of XRD patterns near 14, 29 and 32 degrees.

As it can be seen, all these films exhibit very similar diffraction spectra except several subtle differences. The strong peaks at 14.43, 28.76 and 32.21 degrees are observed, which correspond to the

(110), (220) and (310) planes, respectively, confirming the formation of a tetragonal perovskite structure. In particular, DMF-based Film a shows two additional peaks at 12.99 and 38.98 degrees, which are resulted from the diffraction of (001) and (110) lattice planes of unreacted PbI_2 hexagonal polytype. According to the previous report, such residual PbI_2 would lead to the deterioration of the devices' performance because it induces the defects and exhibits a poor light absorption [37]. Different from DMF, the strong coordinative solvent DMSO results in the formation of the PbI_2–DMSO complex and the retardation crystallization, thus leading to a complete conversion of PbI_2 to $MAPbI_3$ [34]. Therefore, there is no impurity peak observed in the XRD patterns of all DMSO-based films, and the result is consistent with the previous reports [38,33]. The dosage of $PbCl_2$ additive does not alter the crystalline structure, which is indicated by the identical diffraction-peak position of Film b-g. While, comparing closely the diffraction peaks at a certain 2 theta of each film, the subtle differences in strength and width of the peak can be observed; this suggests the crystal domain size and preferred orientation are changed [1] with the amount of doping $PbCl_2$. By comparison, Film d (obtained with 30 mol % $PbCl_2$) appears to show the narrowest diffraction peaks at 14.43 and 28.76 degrees (Figure 1b), indicating a long-range crystalline domains and a high orientation. In addition, it is noticed there are a few minor distinct diffraction peaks in the patterns of Film g, which is due to the fact that it is a very thin one and the substrate might even be exposed (this is proved by SEM images; the reason will be discussed below), thus some interfering peaks derived from the other substances on the substrate might be induced and exhibited. The XRD measurement was also implemented to confirm the phase of nanocrystalline TiO_2 contact layer, and the results presented in ESI indicates a rutile phase of TiO_2 (see Figure S1), which is consist with that reported by literature 36.

Surface morphology and UV–vis absorption

The morphology of perovskite films and its light absorption is crucial to the resultant PSCs' performance, so SEM and UV–vis spectrometry were implemented to investigate the effects on these properties of $MAPbI_3$ films prepared with the various dosage of $PbCl_2$ additive. All the films were fabricated on FTO substrates coated by NRT layer, whose top-view SEM images are presented in Figure 2a–f (the high-magnification images are showed in ESI, Figure S2a-f).

As it shows, the pure PbI_2 solution leads to a film with bad quality as many little cracks bestrew its surface (Figure 2a). Doping with a small amount of $PbCl_2$ (10 mol %), the film surface tends to be rough with the emergence of larger-sized crystal grains, while the cracks are still there (Figure 2b). When $PbCl_2$ additive is doped with an amount of 30 mol %, surprisingly and interestingly, the qualities of the resulted perovskite films are significantly improved (Figure 2c). There are almost no any cracks, while they still exhibit a better uniformity and some crystal grains appear with a size exceeding 500nm. As for the reason why such improvements appear, we consider that it is similar to what Tidhar *et al.* have revealed in the case of chloride inclusion in DMF system [31]. The inactive $PbCl_2$ doped in PbI_2 precursor solution forms heterogeneous nanocrystals which act as a nucleation center, thus a plenty of small perovskite crystals are developed. During the annealing process, the small crystals coalesce to yield large interconnected crystalline domains with high uniformity. The more experiments indicate that the uniformity of the resultant $MAPbI_3$ films is in decline with increasing the dosage of $PbCl_2$ additive (from 50 to 70 and 90 mol %) (Figure 2d-f). This is most likely due to the reason that the more $PbCl_2$ additive means the less PbI_2 precursor (with a total molar concentration of 1 M), which leads to a thinner perovskite film and its uniformity is hard to guarantee. The cross-section SEM images of solar cells based on these films indicate that, Film g (as well as Film f) is with a thickness less than 200nm, and distinctly thinner than Film a-c (more than 300nm, see Figure S3 in ESI), confirming the authenticity of the speculation.

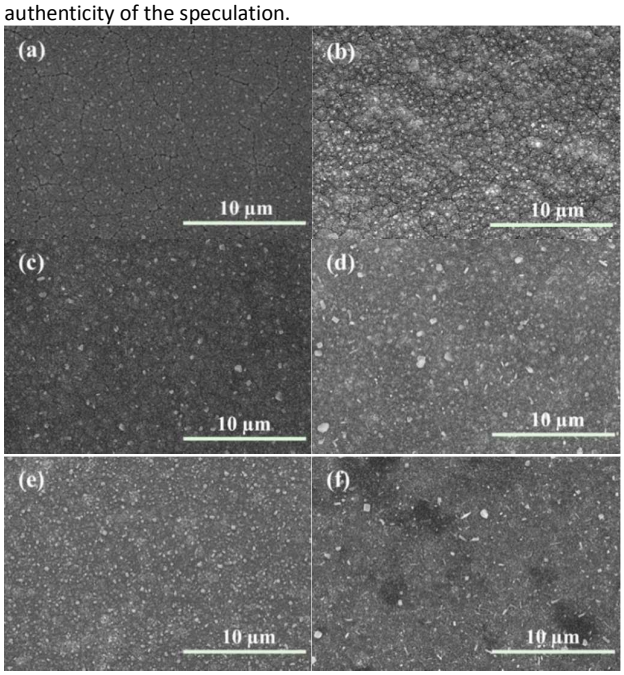

Fig. 2 Top view SEM images of DMSO-based perovskite films prepared with (a) no, (b) 10 mol %, (c) 30 mol %, (d) 50 mol %, (e) 70 mol % and (f) 90 mol % $PbCl_2$ additive, which correspond to as-above mentioned Film b, c, d, e, f and g, respectively.

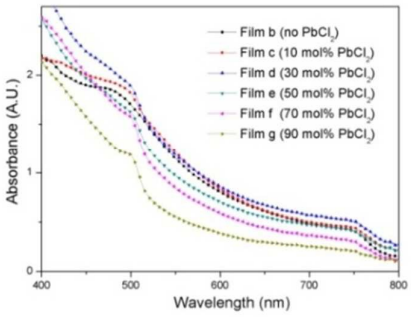

Fig. 3 UV-vis spectra for DMSO-based perovskite films prepared with varying dosage of $PbCl_2$ additive.

Figure 3 shows the UV-vis spectra of DMSO-based perovskite films. All these films present an absorption onset at ~790 nm and the optical band gap is ~1.5 eV (calculated by analysis of the Tauc plots

for direct band gap materials), in agreement with previous measurements [25]. Meanwhile, the light absorption of the films changes with the varying dosage of $PbCl_2$ additive, and this can be explained rationally according to their morphology properties as mentioned above. As it shows, Film b-d exhibit the comparable light absorption properties over the spectral range from 500 to 800 nm. Specifically, Film d exhibits a little bit better than Film b and c, which partly attribute to its enhanced quality; besides, its larger crystal grains would facilitate the stronger light scattering, thus leading to more light absorption especially in long wavelength region. As for Film e-g, the capability of light absorption is deteriorated distinctly and in decline, which is due to the very thin $MAPbI_3$ film with bad uniformity resulted from less PbI_2 precursor and the lower solubility of $PbCl_2$ in DMSO.

We also investigate the morphology of NRT films via SEM measurements. By hydrolyzing an aqueous solution of $TiCl_4$ (200 mM), a NRT film was deposited onto the FTO-coated glass substrates, whose SEM images are shown in Figure 4. It is clearly observed that, the NRT film exhibits a loose structure with good interconnectivity of the TiO_2 nanoparticles, which facilitates the formation of intimate junction of large interfacial area with $MAPbI_3$ and collects photogenerated electrons more effectively. That is to say, it functions as a scaffold and selective contact layer simultaneously, not only facilitates the formation of high quality perovskite films but also acts as contact layer. Moreover, its high surface coverage partitions FTO and $MAPbI_3$ thoroughly, avoiding the deterioration performance resulted by the direct contact them.

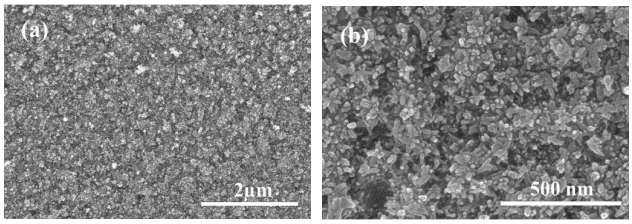

Fig. 4 Top view SEM images of NRT film. (a) and (b) are an image with low and high magnification, respectively.

Evaluation of photovoltaic performance

Employing DMSO-based PbI_2 precursor solution with varying dosage of $PbCl_2$ additive, the PSCs with structure FTO/NRT/$MAPbI_3$/Spiro-MeOTAD/Au were fabricated. We list the performance data of these devices in Table 2, and the *J-V* curves of each champion cell prepared by using a given precursor solution are shown in Figure 5. The devices based on pure PbI_2 precursor are considered as the reference sample, achieving a V_{OC} of 0.97 V, a J_{sc} of 17.6 mA cm^{-2} and a fill factor (FF) of 0.62. Such a performance is comparable with those reported in literature 34, which employed DMSO-based PbI_2 precursor to fabricate the perovskite films on compact TiO_2 coated substrates. As the experiments revealed, despite the pure PbI_2 precursor leads to a perovskite film with better light absorption, it exhibits an inferior film quality. Those cracks on the surface of $MAPbI_3$ films not only induce a mass of defects, but also might cause the direct contact between NRT layer and HTL (spiro-OMeTAD), which will inevitably result in the recombination of carriers and thus lead to a poor performance of the devices. As for the cells based on the precursor with 10 mol % $PbCl_2$ additive, they perform a little better than those no $PbCl_2$ doping. The PCE improvements are benefit from the change of the morphology of $MAPbI_3$ films. As SEM images show (Figure 2b), although the cracks still appear, they tend to be narrower and less than the case of pure PbI_2, which would reduce the number of defects and alleviate the recombination, thus both of V_{OC}, J_{sc} as well as FF increase slightly. Blending 30 mol % $PbCl_2$ into PbI_2 solution of DMSO, the as-prepared solar cells achieve the highest PCE of 14.42%, with a V_{OC} of 1.04 V, a J_{sc} of 20.7 mA cm^{-2} and a FF of 0.67. Compared with the reference samples (those prepared by using pure PbI_2 precursor), the increase percentage of PCE, V_{OC}, J_{sc} and FF is 34.7%, 7.2%, 17.6% and 7.5%, respectively. These remarkable enhancements of performance can be explanted reasonably according the experiment data about the characteristics of the resulted perovskite films. Firstly, 30 mol % $PbCl_2$ additive lead to the almost crack-free $MAPbI_3$ films with larger crystal grains but high uniformity, enhancing light absorption and reducing electrons recombination. Besides, under the condition of doping $PbCl_2$ with a dosage of 30 mol %, the resulted film shows a long-range crystalline domains and a high orientation (as discussed above), which also facilitate the transport of carriers, thus retarding the recombination and achieving a higher J_{sc}. Using the precursor with 50 mol % $PbCl_2$, as-prepared solar cells exhibit the declining J_{sc} and FF, while V_{OC} remains the highest value of 1.04 V. This mainly results from increasing the resistivity of perovskite film with excess chloride doping [21,32], which renders the equivalent series resistance of solar cells increased, so causing the decreases both of J_{sc} and FF, while without impacting V_{OC}. The amount of $PbCl_2$ additive is further increased to 70 and 90 mol %, the device performances are on a distinct downward trend, owing to the deterioration of the perovskite films' uniformity and capability of light harvesting for the reasons as discussed above.

Meanwhile, the employing of NRT layers also play an active role, which contribute to a fabrication process of the photovoltaic device at low temperature; what's more, its loose structure contributes to the formation of perovskite films and leads to an intimate junction of large interfacial area with the $MAPbI_3$, extracting photogenerated electrons more effectively [36]. Finally, it should be noted that our cells exhibit a distinct hysteresis issues when they were measured (see Figure S4 in ESI). Although the origin of hysteresis is still open to debate, it could be overcome by proper interface modification and, to a certain extent, morphology optimization notwithstanding the type of device architecture [39].

Table 2. Performance data of PSCs prepared by varying dosage of $PbCl_2$ additive.

Dosage of $PbCl_2$ (mol %)	V_{OC} (V)	J_{sc} (mA cm^{-2})	FF	PCE [a] (average [b]) (%)
0	0.97	17.6	0.62	10.58 (9.91)
10	0.99	18.2	0.64	11.53 (10.64)
30	1.04	20.7	0.67	14.42 (13.35)
50	1.04	20.3	0.62	13.09 (11.78)
70	0.92	15.8	0.55	7.99 (7.27)
90	0.86	14.47	0.52	6.47 (5.93)

[a] The highest PCE among 12 devices; [b] Average PCE of 12 devices

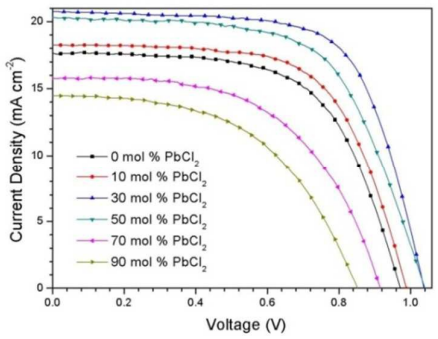

Fig. 5 *J-V* characteristics of the champion cells prepared with varying dosage of $PbCl_2$ additive.

Conclusions

DMSO-based PbI_2 precursor solution with $PbCl_2$ additive was proposed to fabricate $MAPbI_3$ films via sequential solution deposition process. The effects with varying dosage of $PbCl_2$ on the properties of the resultant perovskite films, as well as the cells' performance were investigated. The experimental results indicate that $PbCl_2$ additive strongly affects its morphology and light absorption properties, as well as exhibiting high crystal plane orientation and long-range crystalline domains; while its crystalline structure is not be altered. Under the condition of doping 30 mol % $PbCl_2$ additive, the champion cell achieved a PCE as high as 14.42%, with a J_{sc} of 20.7 mA cm^{-2}, a V_{OC} of 1.04 V and a FF of 0.67, which was significantly improved compared with the top one that prepared by using pure PbI_2 precursor solution. We owe such performance improvements of the devices to the combination of DMSO solvent and chlorine incorporation, which lead to a better quality perovskite films with enhanced capability of light absorption. In addition, the employment of NRT contact layer is very significant due to facilitating the fabrication of the cells at low temperature; also, it promotes the formation of the perovskite films and collects the photogenerated electrons more effectively. This work suggests a simple, low-cost but effective approach to improve the PCE of the PSCs, and we expect that even greater performance enhancement can be achieved through further optimization as revealed.

Acknowledgements

This work is supported partially by National High-tech R&D Program of China (863 Program, No. 2015AA034601), National Natural Science Foundation of China (Grant nos. 91333122, 51402106, 51372082, 51172069, 50972032, 61204064 and 51202067), Ph.D. Programs Foundation of Ministry of Education of China (Grant nos. 20110036110006, 20120036120006, 20130036110012), Par-Eu Scholars Program and the Fundamental Research Funds for the Central Universities.

Notes and references

1. M. M. Lee, J. Teuscher, T. Miyasaka, T. N. Murakami and H. J. Snaith, *Science*, 2012, **338**, 643–647.
2. S. D. Stranks, G. E. Eperon, G. Grancini, C. Menelaou, M. J. P. Alcocer, T. Leijtens, L. M. Herz, A. Petrozza and H. J. Snaith, *Science*, 2013, **342**, 341–344.
3. G. Xing, N. Mathews, S. Sun, S. S. Lim, Y. M. Lam, M. Grätzel, S. Mhaisalkar and T. C. Sum, *Science*, 2013, **342**, 344–347.
4. C. Wehrenfennig, G. E. Eperon, M. B. Johnston, H. J. Snaith and L. M. Herz, *Advanced materials*, 2014, **26**, 1584–1589.
5. S. D. Wolf, J. Holovsky, S. Moon, P. Löper, B. Niesen, M. Ledinsky, F. Haug, J. Yum and C. Ballif, *J. Phys. Chem. Lett.*, 2014, **5**, 1035–1039.
6. N. J. Jeon, J. H. Noh, W. S. Yang, Y. C. Kim, S. Ryu, J. Seo and S. Il Seok, *Nature*, 2015, **517**, 476–480.
7. W. S. Yang, J. H. Noh, N. J. Jeon, Y. C. Kim, S. Ryu, J. Seo and S. I. Seok, *Science*, 2015, **348**, 1234-1237.
8. J. Burschka, N. Pellet, S.-J. Moon, R. Humphry-Baker, P. Gao, M. K. Nazeeruddin and M. Grätzel, *Nature*, 2013, **499**, 316–319.
9. W. Ke, G. Fang, J. Wan, H. Tao, Q. Liu, L. Xiong, P. Qin, J. Wang, H. Lei, G. Yang, M. Qin, X. Zhao and Y. Yan *Nat. Commun.*, 2015, **6**, 1–7.
10. F. Huang, Y. Dkhissi, W. Huang, M. Xiao, I. Benesperi, S. Rubanov, Y. Zhu, X. Lin, L. Jiang, Y. Zhou, A. Gray-Weale, J. Etheridge, C. R. McNeill, R. a. Caruso, U. Bach, L. Spiccia and Y.-B. Cheng, *Nano Energy*, 2014, **10**, 10–18.
11. J.-H. Im, J. Luo, M. Franckevičius, N. Pellet, P. Gao, T. Moehl, S. M. Zakeeruddin, M. K. Nazeeruddin, M. Grätzel and N.-G. Park, *Nano Lett.*, 2015, **15**, 2120–2126.
12. H.-L. Hsu, T.-Y. Juang, C.-P. Chen, C.-M. Hsieh, C.-C. Yang, C.-L. Huang and R.-J. Jeng, *Sol. Energy Mater. Sol. Cells*, 2015, **140**, 224–231.
13. T. Minemoto and M. Murata, *Sol. Energy Mater. Sol. Cells*, 2015, **133**, 8–14.
14. Z. Zhang, D. Wei, B. Xie, X. Yue and M. Li, *Sol. ENERGY*, 2015, **122**, 97–103.
15. P. Cui, P. Fu, D. Wei, M. Li, D. Song and X. Yue, *RSC Adv.*, 2015, **5**, 75622–75629.
16. D. Song, P. Cui, T. Wang, D. Wei, M. Li, F. Cao, X. Yue, P. Fu, Y. Li, Y. He, B. Jiang and M. Trevor, *J. Phys. Chem. C*, 2015, **119**, 22812–22819.
17. H. Zhou, Q. Chen, G. Li, S. Luo, T. -b. Song, H.-S. Duan, Z. Hong, J. You, Y. Liu and Y. Yang, *Science*, 2014, **345**, 542–546.
18. H.-B. Kim, H. Choi, J. Jeong, S. Kim, B. Walker, S. Song and J. Y. Kim, *Nanoscale*, 2014, **6**, 6679–6683.
19. G. E. Eperon, V. M. Burlakov, P. Docampo, A. Goriely and H. J. Snaith, *Adv. Funct. Mater.*, 2014, **24**, 151–157.
20. Y. Zhao and K. Zhu, *J. Phys. Chem. C*, 2014, **118**, 9412–9418.
21 P. Docampo, F. Hanusch, S. D. Stranks, M. Döblinger, J. M. Feckl, M. Ehrensperger, N. K. Minar, M. B. Johnston, H. J. Snaith and T. Bein, *Adv. Energy Mater.*, 2014, **4**, 1–6.
22. C. Zuo and L. Ding, *Nanoscale*, 2014, **6**, 9935–9938.
23. P. W. Liang, C. Y. Liao, C. C. Chueh, F. Zuo, S. T. Williams, X. K. Xin, J. Lin and A. K. Y. Jen, *Adv. Mater.*, 2014, **26**, 3748–3754.
24. Y. Ma, L. Zheng, Y.-H. Chung, S. Chu, L. Xiao, Z. Chen, S. Wang, B. Qu, Q. Gong, Z. Wu and X. Hou, *Chem. Commun.*, 2014, **50**, 12458–12461.
25. Y. Li, J. K. Cooper, R. Buonsanti, C. Giannini, Y. Liu, F. M. Toma and I. D. Sharp, *J. Phys. Chem. Lett.*, 2015, **6**, 493– 499.
26. Q. Chen, H. Zhou, Y. Fang, A. Z. Stieg, T.-B. Song, H.-H. Wang, X. Xu, Y. Liu, S. Lu, J. You, P. Sun, J. McKay, M. S. Goorsky and Y. Yang, *Nat. Commun.*, 2015, **6**, 7269.
27. J. You, Z. Hong, Y. M. Yang, Q. Chen, M. Cai, T. Song, C. Chen, S. Lu, Y. Liu, H. Zhou and Y. Yang, *ACS Nano*, 2014, **8**, 1674–1680.
28. H. Yu, F. Wang, F. Xie, W. Li, J. Chen and N. Zhao, *Adv. Funct. Mater.*, 2014, **24**, 7102–7108.

29. S. Colella, E. Mosconi, P. Fedeli, A. Listorti, F. Orlandi, P. Ferro, T. Besagni, A. Rizzo, G. Calestani, G. Gigli, F. De Angelis, R. Mosca and F. Gazza, *Chem. Mater.*, 2013, **25**, 4613–4618.
30. S. T. Williams, F. Zuo, C.-C. Chueh, C.-Y. Liao, P.-W. Liang and A. K.-Y. Jen, *ACS Nano*, 2014, **8**, 10640–10654.
31. Y. Tidhar, E. Edri, H. Weissman, D. Zohar, G. Hodes, D. Cahen, B. Rybtchinski and S. Kirmayer, *J. Am. Chem. Soc.*, 2014, **136**, 13249–13256.
32. S. Dharani, H. A. Dewi, R. R. Prabhakar, T. Baikie, C. Shi, D. Yonghua, N. Mathews, P. P. Boix and S. G. Mhaisalkar, *Nanoscale*, 2014, **6**, 13854–13860.
33. Q. Chen, H. Zhou, Z. Hong, S. Luo, H.-S. Duan, H.-H. Wang, Y. Liu, G. Li and Y. Yang, *J. Am. Chem. Soc.*, 2013, **136**, 622–625.
34. Y. Wu, A. Islam, X. Yang, C. Qin, J. Liu, K. Zhang, W. Peng and L. Han, *Energy Environ. Sci.*, 2014, **7**, 2934–2938.
35. N. J. Jeon, J. H. Noh, Y. C. Kim, W. S. Yang, S. Ryu and S. Il Seok, *Nature Materials*, 2014, **13**, 897–903.
36. A. Yella, L. P. Heiniger, P. Gao, M. K. Nazeeruddin and M. Grätzel, *Nano Lett.*, 2014, **14**, 2591–2596.
37. Y. Zhao, A. M. Nardes and K. Zhu, *Faraday Discuss.*, 2014, **176**, 301–312.
38. T. Baikie, Y. Fang, J. M. Kadro, M. Schreyer, F. Wei, S. G. Mhaisalkar, M. Graetzel and T. J. White, *J. Mater. Chem. A*, 2013, **1**, 5628–5641.
39. T. Salim, S. Sun, Y. Abe, A. Krishna, A. C. Grimsdale and Y. M. Lam, *J. Mater. Chem. A*, 2015, **3**, 8943–8969.